Supporting Information: Nuclear Quantum Effects Have a Significant Impact on UV/Vis Spectra of Chromophores in Water

Shota Tsuru,*,† Bikramjit Sharma,‡ Christof Hättig,‡ and Dominik Marx‡

†*RIKEN Center for Computational Science, RIKEN, Minatojima-minami 7-1-26, 650-0047, Kobe, Japan*

‡*Lehrstuhl für Theoretische Chemie, Ruhr-Universität Bochum, 44780, Bochum, Germany*

E-mail: shota.tsuru@riken.jp

Contents

1 Computational Methods **3**

1.1 Structural Sampling of Indole in the Gas and Liquid Phases with Classical and Quantum Nuclei 3

1.2 Indole–Water Hydrogen Bonding and Nuclear Quantum Effects 5

1.3 Excitation Energy Calculation and Spectral Simulation 7

1.4 Construction of the Calculated Spectra 8

2 Supplementary Analyses **9**

2.1 Configuration Characters of Vertical Excitations 9

2.2 Computational Spectrum Based on Classical Sampling 12

2.3 Convergence of Spectrum Based on PIQTB Snapshots 12

2.4 Convergence of Spectrum with Respect to Solvation Model 13

2.5 Level Inversion between Excited States due to Solute–Solvent Interaction 17

References **19**

1 Computational Methods

1.1 Structural Sampling of Indole in the Gas and Liquid Phases with Classical and Quantum Nuclei

The structural samplings of indole in the gaseous and solvated states with classical nuclei (will be referred as ab initio molecular dynamics "AIMD" simulations[1]) were performed in the constant temperature ensemble (NVT) at 300 K on the potential energy surface according to the RPBE[2] density functional together with the D3 dispersion correction[3] (using as usual only the two-body terms and zero damping). The Quickstep module[4] for electronic structure calculations within the CP2K package[5,6] used for the AIMD simulations. A TZV2P Gaussian basis set with core electron represented by Goedecker-Teter-Hutter pseudopotentials[7–9] and a plane wave basis representation of the valence density using a kinetic energy cut-off of 500 Ry were employed for the electronic structure calculations underlying all canonical simulations. The temperature of the systems was maintained at an average of 300 K using massive Nosé-Hoover chain[10] thermostat. The gas-phase sampling was performed for 400 ps with the indole molecule within a cubic box of length 18.3667 Å (see text in the next paragraph for choice of this box-length).

To set up the simulations of indole in bulk water, pre-parameterized force field molecular dynamics (FFMD) simulations were performed by employing the OPLS force field[11] for indole and the TIP4P/2005 water model.[12] The FFMD simulations were started using the Gromacs package[13–15] in the constant pressure NpT ensemble at 300 K and 1 atm pressure containing one indole molecule and 600 water molecules (will be referred to as $\mathrm{FFMD_{large}}$) to determine the box length. The pressure and temperature was maintained by Parrinello-Rahman barostatting[16] and canonical sampling through velocity rescaling thermostatting,[17] respectively. The obtained average box length of 26.3228 Å was used for a subsequent NVT simulation of $\mathrm{FFMD_{large}}$ for another 1 ns. Because this relatively large system provides an internal reference with respect to system size smaller systems can be gauged as to proper

solvation of the solute species in water. The radial distribution function (RDF) (Figure S1) between the N-H atom of indole (NH) and oxygen atom of water (OW) atoms from the FFMD NVT trajectory sets the benchmark for reducing the number of water molecules for subsequent AIMD simulations. The number of water molecules were then varied, and it was found that 200 water molecules around indole within a cubic box of dimensions 18.3667 Å subject to periodic boundary conditions perfectly reproduced the NH-OW RDF obtained in the large reference system (Figure S1). Thus, AIMD simulations of one indole in 200 water molecules were launched using this box length. The total length of the AIMD trajectory was 410 ps for indole in water considering the first 10 ps as the equilibration phase. This cubic box length was maintained for AIMD sampling of gas-phase indole as mentioned in the above paragraph.

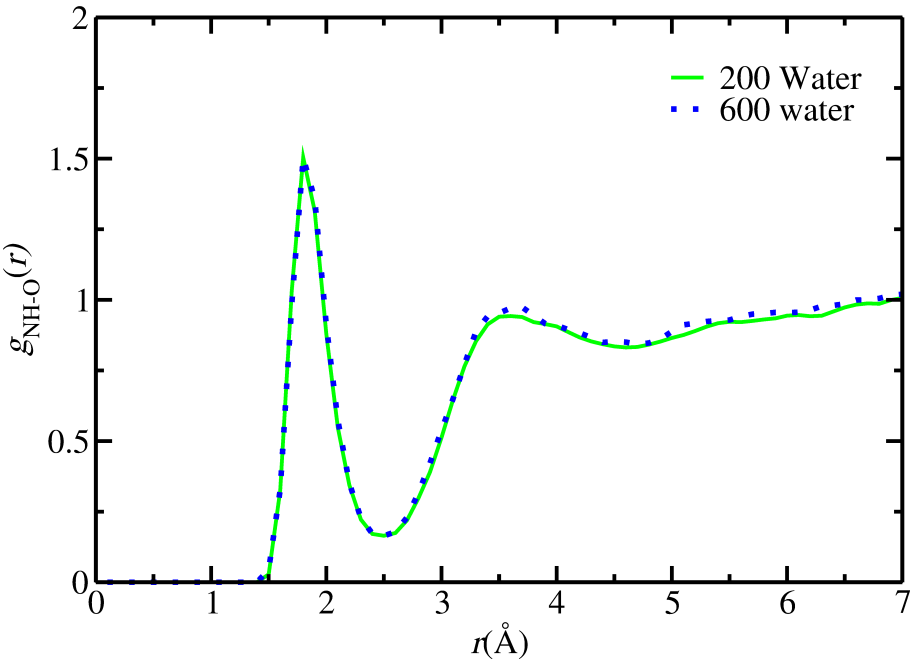


Figure S1: Comparison of NH-O radial distribution functions from force field molecular dynamics of one indole in 600 and 200 water molecules at 300 K. Because it reproduced the solvation structure obtained with 600 water molecules, the system with 200 water molecules was used for all subsequent ab initio simulations using either classical or quantum nuclei.

To include nuclear quantum effects, NQEs, the same simulation set-up (as explained in the first paragraph of this section) was employed for conducting ab initio simulations based

on the rigorous path integral quantum thermal bath, PIQTB, technique[18,19] of indole in gas phase and aqueous solution with 8 Trotter replica (path integral "beads"). The equation of motions for the propagation of classical and quantum nuclei were integrated with time steps of 0.5 and 0.25 fs, respectively. For indole in water, 10 independent snapshots were extracted from the AIMD trajectory with classical nuclei after every 10 ps and 10 independent PIQTB simulations were launched for each of length 20 ps after 2 ps of equilibration, adding up to a total PIQTB sampling time of 200 ps. Snapshots were extracted every 100 fs from each of the trajectories to perform quantum chemical computations of UV/Vis absorption spectra, see below, which were all based on 4000 individual configurations each; in case of the PIQTB simulations each half of the configurations came from beads number 1 and 5, to reduce the correlations along imaginary time.

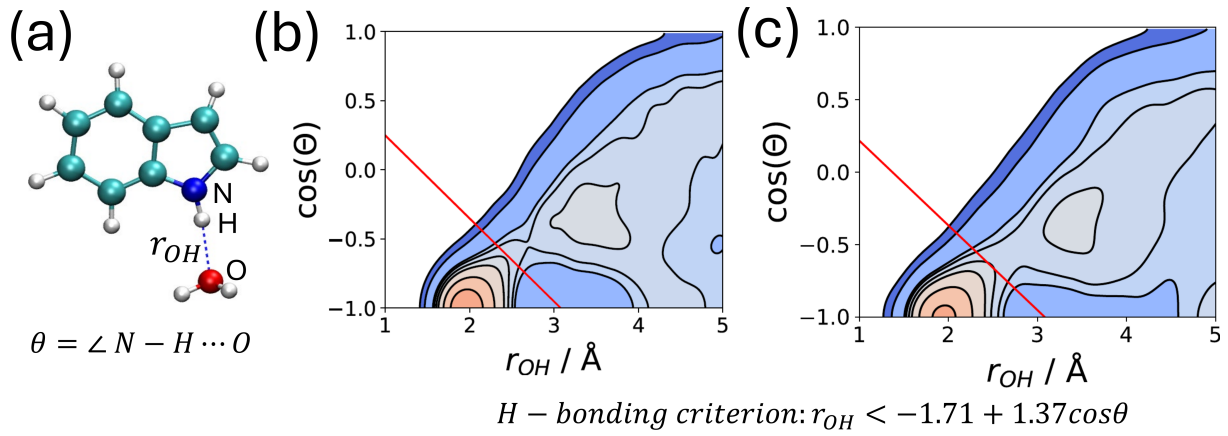


Figure S2: (a) Geometric parameters used for the definition of NH $\cdots$ O hydrogen bonding. Joint probability distributions of $\cos(\theta)$ and r_{OH} for NH $\cdots$ O hydrogen bonding with (b) classical, (c) quantum treatments of nuclei. The region below the red separatrix in each case represent $r_{\mathrm{OH}} < -1.71\cos(\theta) + 1.37$ i.e. NH $\cdots$ O hydrogen bonding.

1.2 Indole–Water Hydrogen Bonding and Nuclear Quantum Effects

A geometric criterion was adopted for defining hydrogen bonding between indole NH and water oxygen (O). The distance between NH and O (r_{OH}) and the cosine of the angle (θ)

formed by the $\mathrm{N-H\cdots O}$ moiety (Figure S2(a)) were involved in the definition of hydrogen bonds. In the joint probability distributions of r_{OH} and $\cos(\theta)$ for classical (Figure S2(b)) and quantum (Figure S2(c)) nuclei trajectories regions could be divided into hydrogen-bonding and non hydrogen-bonding regimes. The hydrogen-bonding region was characterised by high probability of r_{OH} and $\cos(\theta)$ around 2.0 Å and -1.0, respectively. An $\mathrm{N-H\cdots O}$ hydrogen bond was defined if the criterion $r_{\mathrm{OH}} < -1.71\cos(\theta) + 1.37$ was met. Note that the upper limit of this criterion i.e. $r_{\mathrm{OH}} = -1.71\cos(\theta) + 1.37$ defined the separatrix (red line) in each contour. The same criterion nicely captured the hydrogen bonding regions in case of both classical and quantum nuclei trajectories (see Figure S2).

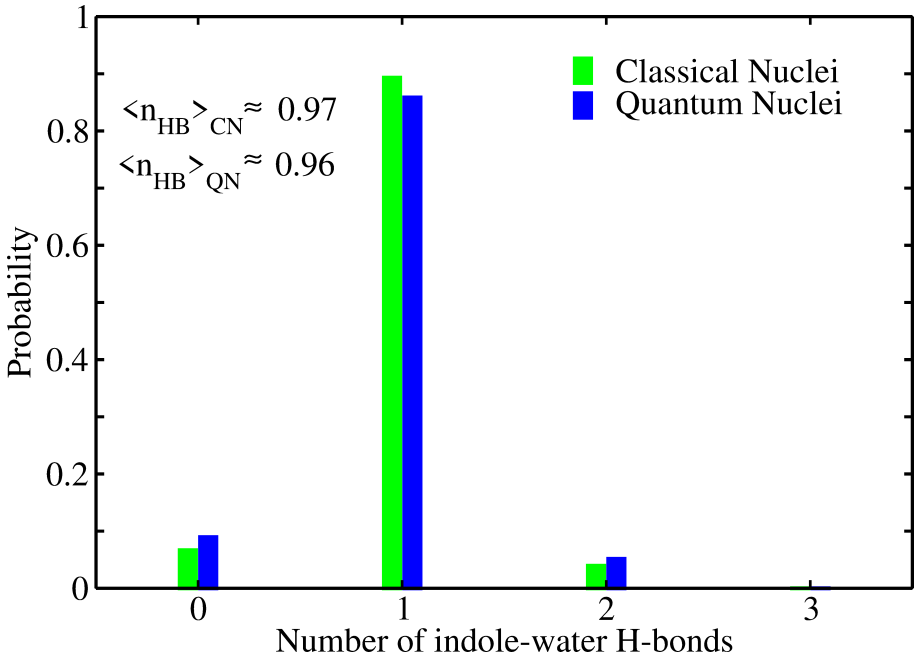


Figure S3: Distribution function of the number of indole-water hydrogen bonds for (green) classical and (blue) PIQTB ensembles. The average numbers of indole-water hydrogen bonds are 0.97 and 0.96 for classical ($\langle n_{HB}\rangle_{CN}$) and quantum ($\langle n_{HB}\rangle_{QN}$) nuclei, respectively.

This also implies that structural quantities, i.e. r_{OH} (enhanced probability around 2.0 Å) and $\cos(\theta)$ (enhanced probability around -1.0) which characterize indole-water hydrogen bonding are not much affected by NQEs on top of the classical thermal fluctuations. This is not unexpected since the intermolecular solvent fluctuations in aqueous solutions at ambient conditions, such as in the present case, are thermally activated which is captured by

classical AIMD. In stark contrast, the intramolecular fluctuations in molecular liquids and solutions are strongly impacted by NQEs which leads to considerable distortions of molecular structures of both solute or solvent species. The negligible impact of the quantum nature of the nuclei on the intermolecular indole-water hydrogen bonding is quantitatively confirmed by the essentially identical hydrogen bond number distributions obtained from the classical AIMD and quantum PIQTB simulations of indole in bulk water according to Figure S3. Notably, they lead to the same average hydrogen bond number of 1.0 (namely 0.97 and 0.96, respectively).

1.3 Excitation Energy Calculation and Spectral Simulation

As described in Sec. 1.1, the ground-state optimized geometry of indole was optimized and vibrational analysis was conducted at the DFT/RPBE-D3/def2-TZVPP level using the ORCA package,[20,21] for consistency with the AIMD simulation. As implemented in SHARC 2.1.,[22] 4000 coordinate sets for the isolated indole molecule were generated according to the Wigner distribution.

For calculating excitation energies for each snapshot of indole in aqueous solution, the indole molecule and the H_2O molecules with hydrogen bond to the N–H group of indole were extracted following the criterion described in Sec. 1.1, and all the other H_2O molecules were replaced by the conductor-like screening model (COSMO).[23] The atomic radii used for construction of the COSMO surface were 2.00, 1.83, 1.72 and 1.30 Å for the carbon, nitrogen, oxygen, and hydrogen atoms, respectively. The COSMO cavity was initially constructed using the atomic radii plus 1.30 Å to the outer solvent spheres and then smoothed at the intersections of the atomic spheres to avoid electrostatic artifacts due to small distances between any cavity centers, as implemented in the TURBOMOLE electronic structure package.[24–26]

Excitation energies for each snapshot were computed using the algebraic-diagramatic construction through second order [ADC(2)] method with the resolution-of-identity (RI)

approximation,[27,28] in conjunction with the aug-cc-pVTZ basis set for indole and the aug-cc-pVDZ basis set[29,30] for H_2O together with the corresponding optimized auxiliary basis sets[31] using the ricc2 program[27,28,32] of TURBOMOLE.[24–26] The typical absolute error at the ADC(2) level is around only 0.1-0.2 eV, whereas those are 0.2-0.4 eV and 0.1-0.3 eV for TDDFT and EOM-CCSD, respectively[33] The number of demanded roots in each calculation was 15 and 8, respectively, in the gas phase and in aqueous solution. These numbers of demanded roots were selected for the highest roots to reach the shortest wavelengths in the energy windows of the spectra measured in the gas phase (6.2 eV)[34] and in aqueous solution (5.4 eV).[35]

The vertical excitation energies were also calculated using (COSMO-)RI-ADC(2) in conjunction with the aug-cc-pVTZ basis set at the ground-state optimized geometry to check the configuration characters and to assign the peaks. For evaluation of quantum-mechanical solute–solvent interactions, the excitation energies were calculated for the 194th snapshot of the bead 5 PIQTB trajectory launched at 10 ps of the AIMD trajectory of indole in water, considering the explicit H_2O molecules within 3.5 Å from any of the atoms forming the indole molecule. All COSMO-RI-ADC(2) calculations employed the post-SCF reaction field coupling scheme[28] with the default cavity and a dielectric constant (ε) of 80.4 and a refractive index (n) of 1.33 for water.

1.4 Construction of the Calculated Spectra

The spectra for ensembles of representative structures were generated by sorting all transitions for all snapshots in the ensemble in histograms with a bin width of 0.05 eV. For each histogram pre-normalized intensity was obtained by summing up the oscillator strengths for all transitions sorted into the respective histogram. Given that the n-th excitation energy calculated for the I-th snapshot was $\omega_{I,k}$ and the oscillator strength of the transition from the ground state to this excited state was $f_{I,k}$, the absorbance of the simulated spectrum

was evaluated in terms of the following histogram,

$$\sigma(\omega) \propto \sum_{I}^{N_{\mathrm{snapshots}}} \sum_{k}^{n_{\mathrm{roots}}} f_{I,k}[\theta(|\omega - \omega_{I,k}| - h_{\mathrm{bin}}/2) + \theta(h_{\mathrm{bin}}/2 - |\omega - \omega_{I,k}|)], \quad (1)$$

where $\theta(\omega)$ denotes the Heaviside step function and $h_{\mathrm{bin}} = 0.05$ eV the bin width. The absorbance $\sigma(\omega)$ was evaluated for bins positioned at $\omega = ...4.625, 4.675, 4.725...$ eV. It should be emphasized that the histograms for all our ensemble spectra (i.e. calculated for the various classial and quantum ensembles in the gas and liquid phases) were calculated using the raw ADC(2) spectra for individual snapshots without shifting or additional broadening. The digitized spectra measured in the gas phase and in aqueous solution were plots of the absorbance in arbitrary unit with respect to the wavelength.[34,35]

Each spectrum was then normalized such that the area under the calculated curve was equal to that under the curve for the measured spectrum in the energy window of 4.0 - 6.2 eV. This scheme was also applied to normalizing each spectrum in aqueous solution, except for the spectrum calculated based on the PIQTB snapshots in aqueous solution removing all the solvent molecule and the experimental spectrum digitized from Ref. 35. In case of the former exception, the intensity was multiplied by $\frac{2}{3}$ after the normalization, because the delayed increase of the second absorption band affected the normalization. In case of the latter exception, whose energy window was truncated at 5.4 eV in the Ref. 35, the intensity was multiplied by 0.6 after the normalization.

2 Supplementary Analyses

2.1 Configuration Characters of Vertical Excitations

Table S1: Energies, oscillator strengths (OSs) and natural transition orbitals (NTOs)[36–39] of the excitations higher than 5.4 eV from the ground state of indole at the ground-state structure in the gas phase (NTO isosurface is 0.02 - 0.035 for Rydberg-type orbitals and 0.05 for others). The value σ denotes the singular values for the NTO pairs, and σ^2 gives relative weight of each NTO pair in the excitation.

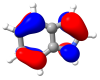
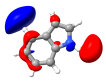
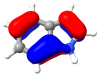
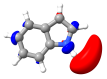
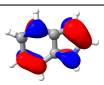
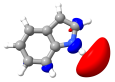
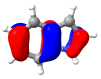
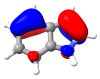
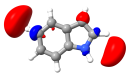
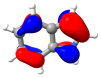
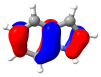
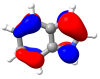
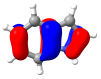
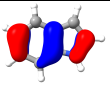
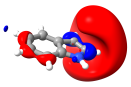
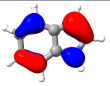
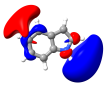
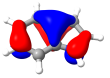
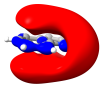
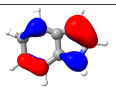
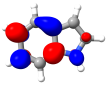
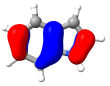
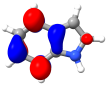
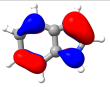
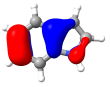
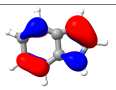
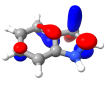
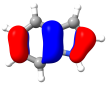
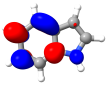
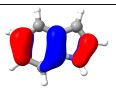
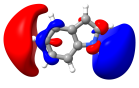
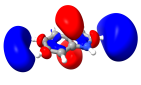
	Energy (eV)	OS	Occupied	σ^2	Virtual
$2A$"	5.52	0.0069		0.92	
				0.08	
$3A$"	5.58	0.0008		0.98	
				0.02	
$4A$"	5.64	0.0004		0.92	
				0.07	
$5A$"	5.95	0.0051		0.98	
				0.02	
$3A'$	6.05	0.6325		0.69	
				0.29	
$4A'$	6.22	0.2250		0.82	
				0.16	

Table S2: Energies, oscillator strengths (OSs) and NTOs of the excitations from the ground state of indole embedded in COSMO higher than 5.4 eV at the ground-state structure (NTO isosurface is 0.018 - 0.036 for Rydberg-type orbitals and 0.05 for others). The value σ denotes the singular values for the NTO pairs, and σ^2 gives relative weight of each NTO pair in the excitation.

	Energy (eV)	OS	Occupied	σ^2	Virtual
$2A$"	5.74	0.0103		0.95	
				0.05	
$3A$"	5.84	0.0012		0.96	
				0.04	
$3A'$	5.86	0.9641		0.70	
				0.28	
$4A$"	5.89	0.0001		0.96	
				0.04	
$4A'$	6.11	0.0722		0.85	
				0.14	
$5A$"	6.28	0.0016		0.87	
				0.12	

2.2 Computational Spectrum Based on Classical Sampling

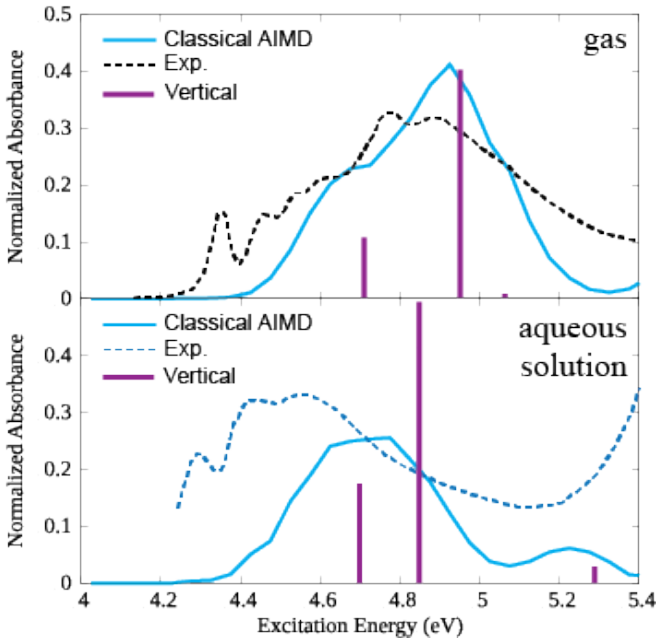


Figure S4: UV/Vis absorption spectrum of indole (upper) in the gas phase and (lower) in aqueous solution, calculated for snapshots from the classical AIMD trajectories, plotted for energy window of 4.0 - 5.4 eV. Dashed black and blue curves are the spectra measured in the gas phase and in aqueous solution, digitized from Refs. 34 and 35, respectively. Curves in the upper panel are common to those in the same colors in Figure 2 of the main manuscript. Purple sticks indicate the calculated vertical spectrum.

2.3 Convergence of Spectrum Based on PIQTB Snapshots

Figure S5 shows UV/Vis absorption spectrum of indole in the gas phase calculated for PIQTB snapshots for beads 1 and 5 and for the combination of the two ensembles. The number of snapshots extracted from each bead is 2000. This assessment demonstrates that the spectrum presented in the main text has sufficiently converged.

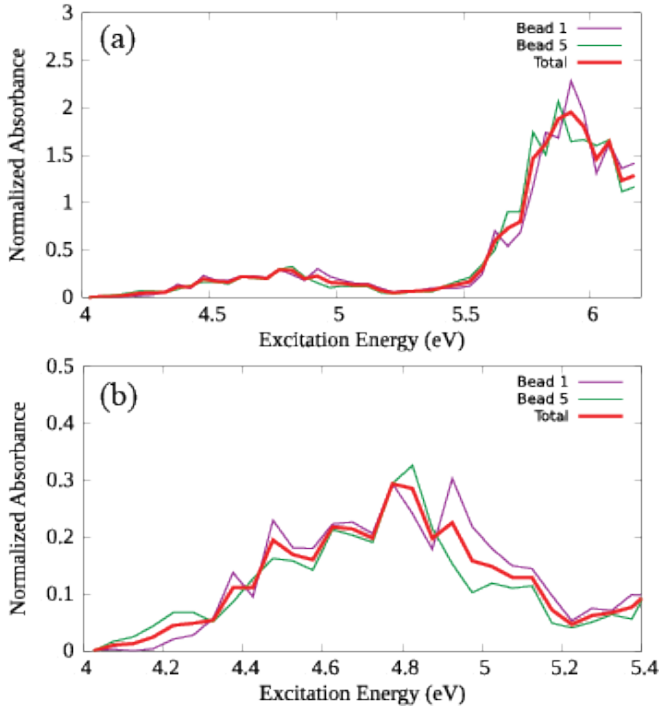


Figure S5: UV/Vis absorption spectrum of indole in the gas phase calculated for PIQTB snapshots from (violet) bead 1, (green) bead 5, and (red) combination of beads 1 and 5, plotted for energy windows of (a) 4.0 - 6.2 eV and (b) 4.0 - 5.4 eV. The red curve is the same as that in the same color in Figure 2 of the main manuscript.

2.4 Convergence of Spectrum with Respect to Solvation Model

Figure S6 shows UV/Vis absorption spectra for indole in aqueous solution based on the snapshots extracted from PIQTB trajectories of indole dissolved in water. The three calculated spectra have been obtained from ADC(2) calculations for the bare indole molecule, indole embedded in COSMO, and a model where indole and explicit water molecules having hydrogen bond to the N–H group of indole embedded in COSMO. The curve calculated for the bare indole molecule indicates that the shape of the spectrum results from distortion of the indole molecule which is sensitive to the solute–solvent interaction, while the peak maxima are reproduced only when the solvent effects on the transitions to the excited states are considered. Further inclusion of explicit water molecules with hydrogen bond to the N–H group of the indole molecule causes only minor changes in the calculated spectrum, and thus

the solvation effects on the transition energies observed in Figure S6 seem to be dominated by electrostatic interaction.

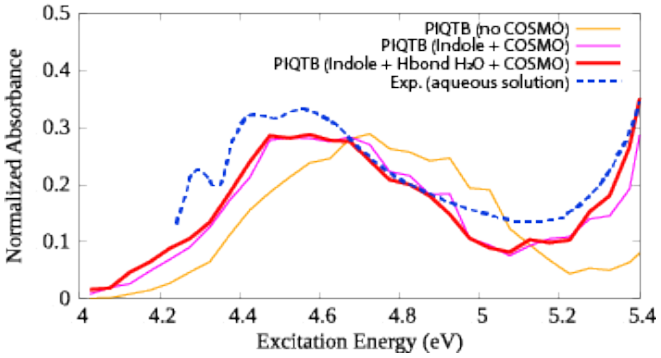


Figure S6: UV/Vis absorption spectra of indole dissolved in water calculated for PIQTB snapshots with solvation models consisting of (orange) only indole molecule, (magenta) indole molecule and COSMO, and (red) indole, explicit water molecules with hydrogen bond to the N–H group, and COSMO. Red curve is same as that in the same color in Figure 3 of the main manuscript. Dashed blue curve is the spectrum measured in aqueous solution digitized from Ref. 35.

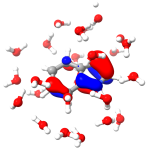
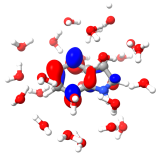
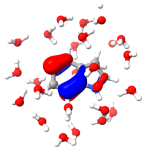
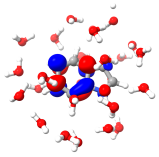
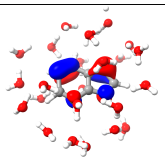
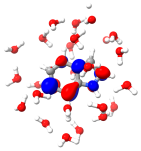
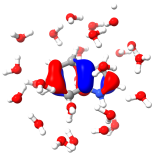
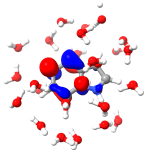
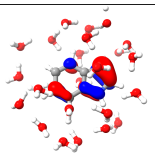
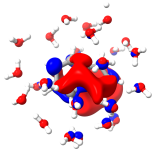
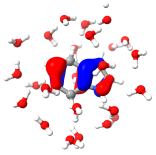
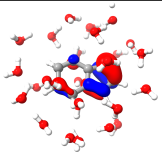
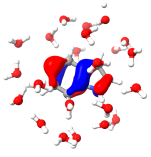
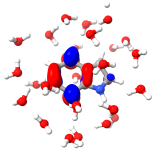
However, replacement of all the solvent molecules with an implicit solvent model like COSMO does not always describe the solvent effects with reasonable accuracy, especially those on Rydberg-type excited states. For more rigorous check of the solvent effects, we chose the 194th snapshot of the bead 5 PIQTB trajectory launched at 10 ps of the AIMD trajectory of indole in water, where the calculations for Figure S6 gives especially large contribution to the band starting at 5.14 eV. The excitation energies and the oscillator strengths were then calculated considering explicit 24 H_2O molecules surrounding the indole molecule and summarized the results in Table S3. NTOs of the four lowest transitions are shown in Table S4, and the dominant virtual NTOs of the third and fourth excitations are visualized in Figure S7 with respect to the number of explicit water molecules. As seen for those of the lowest two $\pi\pi^*$ excitations, inclusion of the explicit 24 H_2O molecules causes only minor changes. Meanwhile, when it comes to the Rydberg-type excitations, it causes blue shift by more than 0.2 eV as a result of distortion of the Rydberg-type orbital like shown in Figure S7. As seen for the S_3 and S_4 states, such blue shift might cause configuration mixing

between Rydberg-type and $\pi\pi^*$ excited states. Therefore, the present reproduction of the UV/Vis absorption spectrum of indole in water utilizing such simple solvation model based on the PIQTB sampling is just a fortunate case due to optical darkness of the Rydberg-type excitations.

Table S3: Excitation energy in eV (and oscillator strength in parenthesis) of each excited state calculated for the 194th snapshot of the bead 5 PIQTB trajectory launched at 10 ps of the AIMD trajectory of indole in water. In each calculation, all the H_2O molecules are replaced with COSMO, those except for the one with hydrogen bond to the N–H group of indole are replaced with COSMO, or those except for 24 H_2O molecules surrounding the indole molecule are replaced with COSMO.

	Indole + COSMO	Indole + 1 H_2O + COSMO	Indole + 24 H_2O + COSMO
S_1	3.92 (0.1305)	3.91 (0.1323)	3.96 (0.1029)
S_2	4.44 (0.0305)	4.43 (0.0291)	4.37 (0.0301)
S_3	4.95 (0.0163)	4.96 (0.0190)	5.17 (0.1475)
S_4	5.28 (0.8334)	5.27 (0.8161)	5.30 (0.5757)
S_5	5.48 (0.0072)	5.49 (0.0165)	5.73 (0.0094)
S_6	5.53 (0.0058)	5.57 (0.0019)	5.76 (0.0273)
S_7	5.63 (0.0243)	5.61 (0.0214)	5.85 (0.0049)
S_8	5.90 (0.0262)	5.88 (0.0211)	5.86 (0.0221)

Table S4: Energies, oscillator strengths (OSs) and NTOs of the excitations from the ground state of indole calculated for the 194th snapshot of the bead 5 PIQTB trajectory launched at 10 ps of the AIMD trajectory of indole in water, where the solvent molecules except for 24 H_2O molecules surrounding the indole molecule are replaced with COSMO. (NTO isosurface is 0.02 for Rydberg-type orbitals and 0.05 for others). The value σ denotes the singular values for the NTO pairs, and σ^2 gives relative weight of each NTO pair in the excitation.

	Energy (eV)	OS	Occupied	σ^2	Virtual
S_1	3.96	0.1029		0.95	
				0.04	
S_2	4.37	0.0301		0.72	
				0.27	
S_3	5.17	0.1475		0.86	
				0.13	
S_4	5.30	0.5757		0.65	
				0.31	

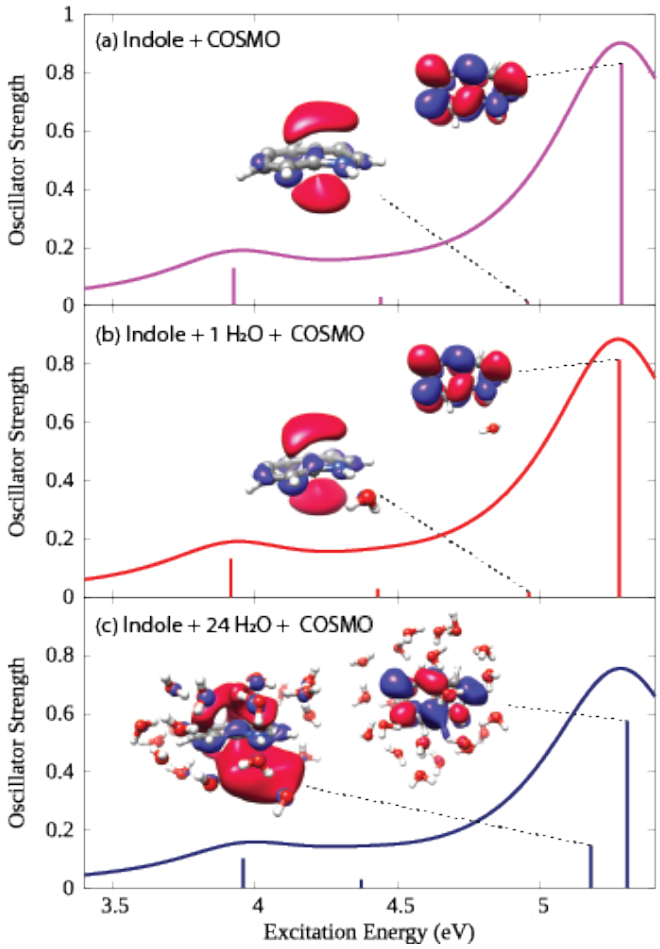


Figure S7: Excitation energies and oscillator strengths calculated for (a) only the indole molecule, (b) indole and a water molecule with hydrogen bond to the N–H group, and (c) indole and surrounding 24 water molecules, at the 194th snapshot of the bead 5 PIQTB trajectory launched at 10 ps of the AIMD trajectory of indole in water. Each microsolvation model is embedded in COSMO. Curve of each panel is obtained by fitting Lorentzian function with full width of half maximum (FWHM) of 0.6 eV to the bars. Orbital pictures in each panels are the dominant virtual NTOs of the excitations to the S_3 and S_4 states.

2.5 Level Inversion between Excited States due to Solute–Solvent Interaction

We discuss the influence of the level inversion between the ^1L_b and ^1L_a states on the UV/Vis spectrum by analyzing the snapshots for the classical AIMD and PIQTB ensembles (used for

Table S5: Number (percentage) of snapshots where level inversion between the ^1L_b and ^1L_a states occurred (oscillator strength of the S_0–S_1 transition is more than 0.10 while 0.0487 and 0.1357 for the ^1L_b and ^1L_a states at the optimized geometry, respectively) among the 4000 snapshots analyzed for each of the four setups (gas phase versus solution and classical versus quantum nuclei).

	^1L_a lower than ^1L_b
Classical AIMD (gas)	60 (1.5%)
PIQTB (gas)	337 (8.4%)
Classical AIMD (solution)	968 (24.2%)
PIQTB (solution)	1600 (40%)

Figure S4 and Figure 3 of the main manuscript, respectively) both in the gas phase and in aqueous solution. Table S5 reports the number and percentage of snapshots where such level inversion occurred, i.e. the oscillator strength of the S_0–S_1 transition is more than 0.10 while 0.0487 and 0.1357 for S_0–S_1(^1L_b) and S_0–S_2(^1L_a) at the optimized geometry, respectively. In the gas phase, we find that level inversion is a minor effect because it is observed for only 8.4% of the snapshots even when NQEs are included. In stark contrast, level inversion effects are very significant in solution: They are observed for 40% of all quantum (PIQTB) snapshots and even important for classical nuclei obtained from AIMD sampling. The observed ^1L_b–^1L_a inversion indicates that a ^1L_b/^1L_a conical intersection lies close to the optimized geometry when the indole molecule is dissolved in water. Since the ensemble approaches do not take account of nonadiabatic effects caused by conical intersections near the optimized geometry, the ^1L_b/^1L_a conical intersection may partially account for the lineshapes missing in the simulated spectrum especially in aqueous solution, as in the case of pyrazine: Lineshape approaches including such nonadiabatic effects by a model vibronic Hamiltonian almost fully reproduced the lineshapes in the UV/Vis absorption spectrum measured for the isolated pyrazine molecule,[40] which was not fully reproduced by an ensemble approach based on Wigner sampling.[41] In this context, solvent effects, including NQEs, may further complicate UV/Vis absorption by shifting conical intersections between excited states.

References

(1) Marx, D.; Hutter, J. Ab Initio Molecular Dynamics: Basic Theory and Advanced Methods; Cambridge University Press, 2009.

(2) Hammer, B.; Hansen, L. B.; Nørskov, J. K. Improved adsorption energetics within density-functional theory using revised Perdew-Burke-Ernzerhof functionals. Phys. Rev. B **1999**, 59, 7413–7421.

(3) Grimme, S.; Antony, J.; Ehrlich, S.; Krieg, H. A consistent and accurate *ab initio* parametrization of density functional dispersion correction (DFT-D) for the 94 elements H-Pu. J. Chem. Phys. **2010**, 132, 154104.

(4) VandeVondele, J.; Krack, M.; Mohamed, F.; Parrinello, M.; Chassaing, T.; Hutter, J. QUICKSTEP: Fast and accurate density functional calculations using a mixed Gaussian and plane waves approach. Comput. Phys. Commun. **2005**, 167, 103–128.

(5) Hutter, J.; Iannuzzi, M.; Schiffmann, F.; VandeVondele, J. CP2K: atomistic simulations of condensed matter systems. WIREs Comput. Mol. Sci. **2014**, 4, 15–25.

(6) Kühne, T. D.; Iannuzzi, M.; Del Ben, M.; Rybkin, V. V.; Seewald, P.; Stein, F.; Laino, T.; Khaliullin, R. Z.; Schütt, O.; Schiffmann, F.; Golze, D.; Wilhelm, J.; Chulkov, S.; Bani-Hashemian, M. H.; Weber, V.; Borštnik, U.; Taillefumier, M.; Jakobovits, A. S.; Lazzaro, A.; Pabst, H.; Müller, T.; Schade, R.; Guidon, M.; Andermatt, S.; Holmberg, N.; Schenter, G. K.; Hehn, A.; Bussy, A.; Belleflamme, F.; Tabacchi, G.; Glöß, A.; Lass, M.; Bethune, I.; Mundy, C. J.; Plessl, C.; Watkins, M.; VandeVondele, J.; Krack, M.; Hutter, J. CP2K: An electronic structure and molecular dynamics software package - Quickstep: Efficient and accurate electronic structure calculations. J. Chem. Phys. **2020**, 152, 194103.

(7) Goedecker, S.; Teter, M.; Hutter, J. Separable dual-space Gaussian pseudopotentials. Phys. Rev. B **1996**, 54, 1703–1710.

(8) Hartwigsen, C.; Gœdecker, S.; Hutter, J. Relativistic separable dual-space Gaussian pseudopotentials from H to Rn. Phys. Rev. B **1998**, 58, 3641–3662.

(9) Krack, M. Pseudopotentials for H to Kr optimized for gradient-corrected exchange-correlation functionals. Theor. Chem. Acc. **2005**, 114, 145–152.

(10) Martyna, G. J.; Klein, M. L.; Tuckerman, M. Nosé–Hoover chains: The canonical ensemble via continuous dynamics. J. Chem. Phys. **1992**, 97, 2635–2643.

(11) Jorgensen, W. L.; Maxwell, D. S.; Tirado-Rives, J. Development and testing of the OPLS all-atom force field on conformational energetics and properties of organic liquids. J. Am. Chem. Soc. **1996**, 118, 11225–11236.

(12) Abascal, J. L. F.; Vega, C. A general purpose model for the condensed phases of water: TIP4P/2005. J. Chem. Phys. **2005**, 123, 234505.

(13) Pronk, S.; Páll, S.; Schulz, R.; Larsson, P.; Bjelkmar, P.; Apostolov, R.; Shirts, M. R.; Smith, J. C.; Kasson, P. M.; van der Spoel, D.; Hess, B.; Lindahl, E. GROMACS 4.5: a high-throughput and highly parallel open source molecular simulation toolkit. Bioinformatics **2013**, 29, 845–854.

(14) Van Der Spoel, D.; Lindahl, E.; Hess, B.; Groenhof, G.; Mark, A. E.; Berendsen, H. J. GROMACS: Fast, flexible, and free. J. Comput. Chem. **2005**, 26, 1701–1718.

(15) Hess, B.; Kutzner, C.; Van Der Spoel, D.; Lindahl, E. GROMACS 4: Algorithms for highly efficient, load-balanced, and scalable molecular simulation. J. Chem. Theory Comput. **2008**, 4, 435–447.

(16) Parrinello, M.; Rahman, A. Polymorphic transitions in single crystals: A new molecular dynamics method. J. Appl. Phys. **1981**, 52, 7182–7190.

(17) Bussi, G.; Donadio, D.; Parrinello, M. Canonical sampling through velocity rescaling. J. Chem. Phys. **2007**, 126, 014101.

(18) Brieuc, F.; Dammak, H.; Hayoun, M. Quantum thermal bath for path integral molecular dynamics simulation. J. Chem. Theory Comput. **2016**, 12, 1351–1359.

(19) Schran, C.; Brieuc, F.; Marx, D. Converged Colored Noise Path Integral Molecular Dynamics Study of the Zundel Cation Down to Ultralow Temperatures at Coupled Cluster Accuracy. J. Chem. Theory Comput. **2018**, 14, 5068–5078.

(20) Neese, F. The ORCA program system. Wiley Interdiscip. Rev. Comput. Mol. Sci. **2012**, 2, 73–78.

(21) Neese, F. Software update: The ORCA program system—Version 5.0. Wiley Interdiscip. Rev. Comput. Mol. Sci. **2022**, 12, e1606.

(22) Mai, S.; Richter, M.; Heindl, M.; Menger, M. F. S. J.; Atkins, A. J.; Ruckenbauer, M.; Plasser, F.; Ibele, L. M.; Kropf, S.; Oppel, M.; et al. SHARC2.1: Surface Hopping Including Arbitrary Couplings – Program Package for Non-Adiabatic Dynamics; available from `sharc-md.org`.

(23) Klamt, A.; Schüürmann, G. COSMO: a new approach to dielectric screening in solvents with explicit expressions for the screening energy and its gradient. J. Chem. Soc., Perkin Trans. 2 **1993**, 799–805.

(24) TURBOMOLE V7.8 2023, a development of University of Karlsruhe and Forschungszentrum Karlsruhe GmbH, 1989-2007, TURBOMOLE GmbH, since 2007; available from
`https://www.turbomole.org`.

(25) Balasubramani, S. G.; Chen, G. P.; Coriani, S.; Diedenhofen, M.; Frank, M. S.; Franzke, Y. J.; Furche, F.; Grotjahn, R.; Harding, M. E.; Hättig, C.; Hellweg, A.; Helmich-Paris, B.; Holzer, C.; Huniar, U.; Kaupp, M.; Marefat Khah, A.; Karbalaei Khani, S.; Müller, T.; Mack, F.; Nguyen, B. D.; Parker, S. M.; Perlt, E.; Rappoport, D.; Reiter, K.; Roy, S.; Rückert, M.; Schmitz, G.; Sierka, M.; Tapavicza, E.;

Tew, D. P.; van Wüllen, C.; Voora, V. K.; Weigend, F.; Wodyński, A.; Yu, J. M. TURBOMOLE: Modular program suite for *ab initio* quantum-chemical and condensed-matter simulations. J. Chem. Phys. **2020**, 152, 184107.

(26) Franzke, Y. J.; Holzer, C.; Andersen, J. H.; Begušić, T.; Bruder, F.; Coriani, S.; Della Sala, F.; Fabiano, E.; Fedotov, D. A.; Fürst, S.; Gillhuber, S.; Grotjahn, R.; Kaupp, M.; Kehry, M.; Krstić, M.; Mack, F.; Majumdar, S.; Nguyen, B. D.; Parker, S. M.; Pauly, F.; Pausch, A.; Perlt, E.; Phun, G. S.; Rajabi, A.; Rappoport, D.; Samal, B.; Schrader, T.; Sharma, M.; Tapavicza, E.; Treß, R. S.; Voora, V.; Wodyński, A.; Yu, J. M.; Zerulla, B.; Furche, F.; Hättig, C.; Sierka, M.; Tew, D. P.; Weigend, F. TURBOMOLE: Today and Tomorrow. J. Chem. Theory Comput. **2023**, 19, 6859–6890.

(27) Hättig, C. Structure optimizations for excited states with correlated second-order methods: CC2, CIS(D∞), and ADC(2). Adv. Quant. Chem. **2005**, 50, 37–60.

(28) Karbalaei Khani, S.; Marefat Khah, A.; Hättig, C. COSMO-RI-ADC(2) excitation energies and excited state gradients. Phys. Chem. Chem. Phys. **2018**, 20, 16354–16363.

(29) Dunning, Jr., T. H. Gaussian basis sets for use in correlated molecular calculations. I. The atoms boron through neon and hydrogen. J. Chem. Phys. **1989**, 90, 1007.

(30) Kendall, R. A.; Dunning, T. H.; Harrison, R. J. Electron-affinities of the 1st-row atoms revisited - systematic basis-sets and wave-functions. J. Chem. Phys. **1992**, 96, 6796–6806.

(31) Weigend, F.; Köhn, A.; Hättig, C. Efficient use of the correlation consistent basis sets in resolution of the identity MP2 calculations. J. Chem. Phys. **2001**, 116, 3175–3183.

(32) Hättig, C.; Weigend, F. CC2 excitation energy calculations on large molecules using the resolution of the identity approximation. J. Chem. Phys. **2000**, 113, 5154–5161.

(33) Loos, P.-F.; Scemama, A.; Jacquemin, D. The Quest for Highly Accurate Excitation Energies: A Computational Perspective. J. Phys. Chem. Lett. **2020**, 11, 2374–2383.

(34) Livingstone, R.; Schalk, O.; Boguslavskiy, A. E.; Wu, G.; Therese Bergendahl, L.; Stolow, A.; Paterson, M. J.; Townsend, D. Following the excited state relaxation dynamics of indole and 5-hydroxyindole using time-resolved photoelectron spectroscopy. J. Chem. Phys. **2011**, 135, 194307.

(35) Kumar, G.; Roy, A.; McMullen, R. S.; Kutagulla, S.; Bradforth, S. E. The influence of aqueous solvent on the electronic structure and non-adiabatic dynamics of indole explored by liquid-jet photoelectron spectroscopy. Faraday Discuss. **2018**, 212, 359–381.

(36) Luzanov, A. V.; Sukhorukov, A. A.; Umanskii, V. É. Application of transition density matrix for analysis of excited states. Theor. Exp. Chem. **1976**, 10, 354–361.

(37) Luzanov, A. V.; Zhikol, O. A. In Practical Aspects of Computational Chemistry; Leszczynski, J., Shukla, M. K., Eds.; Springer: Heidelberg, Germany, 2012; Vol. I; pp 415 – 449.

(38) Martin, R. L. Natural transition orbitals. J. Chem. Phys. **2003**, 118, 4775–4777.

(39) Mayer, I. Using singular value decomposition for a compact presentation and improved interpretation of the CIS wave functions. Chem. Phys. Lett. **2007**, 437, 284–286.

(40) Lambertson, E.; Bashirova, D.; Hunter, K. E.; Hansen, B.; Zuehlsdorff, T. J. Computing linear optical spectra in the presence of nonadiabatic effects on graphics processing units using molecular dynamics and tensor-network approaches. J. Chem. Phys. **2024**, 161, 114101.

(41) Tsuru, S.; Sharma, B.; Marx, D.; Hättig, C. Structural Sampling and Solvation Models

for the Simulation of Electronic Spectra: Pyrazine as a Case Study. J. Chem. Theory Comput. **2023**, 19, 2291–2303.